Journal of Power Sources 185 (2008) 411–418

Contents lists available at ScienceDirect

Journal of Power Sources

journal homepage: www.elsevier.com/locate/jpowsour

Short communication

Aligned carbon nanotube–Pt composite fuel cell catalyst by template electrodeposition

Lorraine C. Nagle, James F. Rohan*

Tyndall National Institute, University College Cork, Lee Maltings, Prospect Row, Cork, Ireland

ARTICLE INFO

Article history:
Received 20 February 2008
Received in revised form 20 May 2008
Accepted 22 June 2008
Available online 4 July 2008

Keywords:
Electrocatalyst
Composite
Template
Methanol
Fuel cell
Microfabricated

ABSTRACT

Solution phase deposition of aligned arrays of carbon nanotubes (CNTs) in a platinum (Pt) matrix composite is demonstrated. The catalyst material is electrodeposited in an oriented manner on the nanoscale using anodised aluminium oxide (AAO) templates. The catalyst performance of the composite for the oxidation of methanol is shown. The carbon monoxide (CO) tolerance is increased and the catalyst function is improved by minimising the influence of adsorbed CO on the kinetics of the methanol oxidation reaction.

1. Introduction

Fuel cells are being investigated world-wide as a power source for portable electronic applications [1]. The fabrication of micro-fuel cells where the active electrode size is limited to the order of cm^2 would benefit from microfabrication compatibility for integration with the microelectronic devices to be powered. Micro-fuel cells may be used to power autonomous microsystems and distributed elements in wireless sensor networks. Several research groups have proposed microfabrication processes for fuel cells using methanol [2,3] and H_2 gas [4–6] as fuel. In these cases the catalyst was not textured or specifically optimised for the microfabricated cell. Indeed for the standard dispersed Pt-based catalysts on high surface area carbon support materials it is not possible to micropattern the catalyst materials for improvements in electrode or full cell layout. The cells are therefore limited by the electrocatalyst material and fabrication route employed. The microfabrication route demonstrated in this work enables a patterned high surface catalyst deposition for the specific case of a direct methanol fuel cell (DMFC). For portable applications the DMFC has the advantage of direct fuel feed to the cell under atmospheric pressure and moderate operating temperatures thereby obviating the need for reformers to convert the fuel to hydrogen before introduction to the active cell compartment. The catalysts of choice for the DMFC are Pt alloys [7] usually with Ru for the methanol oxidation anode and pure Pt for the oxygen reduction cathode. A significant technical hurdle to be addressed is in developing a CO tolerant electrocatalyst for DMFCs. The Ru alloy of Pt has been shown to improve the catalytic reaction by introducing a lower potential for the OH adsorption reaction on the catalyst material which may then react at a higher rate with the adsorbed CO by-product from methanol oxidation to produce CO_2 and an active catalyst for continuous methanol oxidation.

A recent development in the optimisation of precious metal catalyst and high surface area support materials has been the investigation of CNTs [8–10] to replace traditional carbon powders. To improve the utilisation efficiency of Pt catalyst requires finding the optimum material configuration while minimising Pt loading and ensuring electrical continuity. CNTs are believed to be superior to conventional carbon black as a support in that they aid the dispersion of Pt thereby maximising the surface area available for reaction and minimising grain growth. These factors significantly enhance electrocatalytic activity [11]. Pt nanoparticle–CNT composite electrodes are usually prepared by decorating Pt nanoparticles at the surface of CNTs and configuring the composite into a functional electrode. However, it is difficult to attach Pt nanoparticles to the CNT surface through impregnation or deposition owing to the inertness of the CNT walls. To date, the most established route for immobilisation and dispersion of metal particles on CNTs requires generation of functional groups on the external walls by

* Corresponding author. Tel.: +353 214904224; fax: +353 214270271.
E-mail address: james.rohan@tyndall.ie (J.F. Rohan).

0378-7753/$ – see front matter © 2008 Elsevier B.V. All rights reserved.
doi:10.1016/j.jpowsour.2008.06.067

harsh oxidative treatment, followed by chemical or electrochemical deposition of metal on the activated CNT walls. Despite chemical modification it is still difficult to control particle size and deposition of Pt nanoparticles on CNTs. This process frequently results in aggregated Pt particles which in turn lowers the available surface area, decreases the mass activity of the catalyst and may degrade the mechanical and electrochemical electrode performance. Pt catalysts prepared using the chemical reduction method may be compromised by impurities from the bath solutions which can deteriorate catalyst activity. Anchoring Pt nanoparticle–CNT composites on a conducting surface is a crucial step in constructing a robust electrode assembly with low resistivity. This involves casting the treated CNTs onto an electrode surface or dispersing CNTs in a binder (such as *N*,*N*-dimethylformamide or teflon) to form a CNT electrode. However, binders can cause an increase in resistivity. The preparation of such CNT-based electrodes is complicated and may degrade the mechanical and electrochemical performance of the CNT electrode. In that particular electrode assembly type a high contact resistance between Pt nanoparticle–CNT composites and current collectors (graphite foil or metallic substrates) is introduced and an electronic pathway may not be guaranteed. The co-electrodeposition of CNTs and Pt described in this work reinforces CNTs *in* Pt ensuring an electronic pathway.

A second approach is to use chemical vapour deposition (CVD) to grow an aligned array of CNTs directly on a conducting substrate, the CNTs are then decorated with Pt nanoparticles. The decoration of aligned CNTs grown in anodised aluminium oxide (AAO) templates has been demonstrated [12]. This serves to lower the contact resistance between the Pt–CNT composite thus obtained and the substrate. An aligned array of CNTs decorated with Pt nanoparticles offers much improved electrocatalytic performance over that of randomly dispersed Pt–CNTs. The electrical conductivity of CNTs is higher along rather than across the tubes. Tang et al. [13] demonstrated the electrodeposition of Pt nanoparticles on (i) tangled CNTs grown on graphite and (ii) aligned CNTs grown on Ti. Their electrocatalytic activities were compared and the latter was superior for methanol oxidation. However, this approach also suffers from a number of limitations. Electrochemical deposition of nanoparticles on an aligned array of CNTs can result in CNTs moving in the wet processing environment and agglomerating. This misaligns the CNT array and lowers the available surface area of CNTs for subsequent nanoparticle decoration. There is a decrease in available catalytic surface area with time as Pt nanoparticles agglomerate which in turn lowers the mass activity of the catalyst. It is difficult to prepare Pt nanoparticles with a uniform small diameter (<5 nm) at high Pt loading—both critical features of a high-performance catalyst. The adhesion at the CNT–metal nanoparticle interface is not optimal. It can also be difficult to grow aligned CNTs on carbon paper by CVD due to its rough nature.

A number of researchers have presented analysis of CNT composite catalysts with enhanced activity for methanol oxidation. One group reported a tenfold catalytic activity enhancement for methanol oxidation by doping Pt-carbon black catalyst ink with single-walled carbon nanotubes (SWNTs) [14]. They attributed this to the increase of catalyst utilisation by improving interconnectivity among carbon black particles. He and co-workers [15] synthesised ordered mesoporous carbon nanofibers (MCNFs) and ordered mesoporous carbons (OMCs) as supports for loading Pt nanoparticles The electrochemical properties of the two catalysts and the commercial catalyst Pt/C(E-TEK), which is used for comparison, were studied by cyclic voltammetry. The results reveal that the catalyst using MCNFs as support has excellent electrochemical performance for hydrogen and methanol electro-oxidation. The electrochemical active surface of Pt particles for the Pt/MCNFs in sulphuric acid solution reaches a value about four times that of Pt/OMCs and twice that of Pt/C(E-TEK). The Pt/MCNFs catalyst has higher CO tolerance in the methanol solution and exhibits higher activity for methanol electro-oxidation than the other two catalysts. Liang et al. [16] studied the oxidation of methanol at Pt electrocatalysts supported on multi-walled carbon nanotubes (MWNTs) with various diameters and lengths. By comparison with long MWNTs, the short MWNTs had more open ends, resulting in high Pt dispersion and electrocatalytic activity towards methanol oxidation. Pt nanoparticles supported on short MWNTs with a diameter of 30–50 nm exhibited the best Pt dispersion and highest methanol oxidation activity among the catalysts studied. The increased activities of the catalysts based on short MWNTs were attributed to both the intrinsic high activity of the ends of MWNTs and a good Pt distribution. Yang et al. [17] demonstrated high electrocatalytic activity for 3D Pt nanoparticle clusters with a fractal structure obtained by potential step electrodeposition on MWNTs for methanol oxidation. The electrocatalytic activity and stability for methanol oxidation surpassed that at a 2D uniform Pt nanoparticle dispersion on MWNTs obtained by cyclic voltammetry. The enhanced behaviour was assigned to the unique 3D 'flower-like' structure of the Pt nanoparticle clusters on MWNTs with significantly increased electrochemically active surface areas. A further method for CNT and subsequent Pt catalyst deposition has been reported where an electrophoretic deposition technique (40 V for 2–5 min) was utilised [18] to deposit CNTs on a positive electrode from a non-aqueous solvent (Tetrahydrofuran) with the Pt catalyst subsequently deposited on the high surface area substrate. In addition to nanoparticle catalyst deposition on CNT support structures described above, researchers have also loaded the catalyst within the CNT support [19].

To further the case for the incorporation of CNTs as the support material a recent paper has described the use of MWNTs as a sensor for gaseous CO and demonstrated that the overpotential for CO oxidation is lowered by a decrease in the CO adsorption energy on this specific carbon substrate and the oxidation current increased [20]. In alternative application areas researchers have shown the possibility of incorporating CNTs with electrodeposits as a composite for improved wear, hardness, thermal conductivity and field emission characteristics [21–24].

The co-electrodeposition of Pt and CNT described in this work aims at minimising the disadvantages of the composites described above while achieving increased performance for methanol oxidation based on the advantages of this composite material which these researchers have highlighted. This was investigated through the combined use of electrodeposited composite materials and porous templates to confine the deposit and increase the surface area. CNTs may be reversibly solubilised in aqueous solutions through the use of polymers which have been shown to wrap the nanotube [25]. The polymer wrapping of the CNTs leads to individual nanotubes rather than the agglomerates that typically occur in solvents for the unmodified or pristine hydrophobic CNTs by disruption of the strong van der Waals interaction along the length of the nanotubes. It has been suggested that it is this destabilisation of the solid that shifts the equilibrium towards the dissolved phase. Polyacrylic acid has been utilised to assist the dispersion of nanotubes for electrochemical composite deposition. In the case of Cu composites this polymer did not yield smooth, void free composites [26]. The commercial polymer Nafion has also been proposed as a solubilising agent [27]. These researchers indicated that the polymer-wrapped CNTs retained their electrocatalytic activity for hydrogen peroxide in addition to being an effective solubilising agent. Nafion can be considered as a polyelectrolyte when used in aqueous environment and has the ability to introduce a charge at the surface of CNTs that will prevent aggregation after dispersion by repulsive electrostatic forces, similar to the case of nanoparti-

cle dispersions [28]. Another feature of the CNT/Nafion system that may be of benefit in the solubilisation of the CNTs is their possible protonation by interaction with the acidic functionalities of the Nafion leading to local charge transfer interactions with the nanotube to assist the dispersion and solubilisation of the CNTs in the aqueous solvent [29,30].

In this work MWNTs were utilised rather than SWNTs as a support for the Pt catalyst because of the relatively high electrical conductivity which has been attributed to the larger outer shells [31]. MWNTs have multiple 1D conducting shells and their conductance will thus be higher depending on the number of shells. In this work we demonstrate a method to achieve selective Pt–CNT composite catalyst deposition on Si substrates. The introduction of CNT codeposits with the Pt results in improved functionality of the catalyst material deposited. We have utilised commercial Whatman Anodisc® and in-house porous AAO templates to facilitate high surface area catalyst deposition. The in-house AAO may be patterned on Si substrates [32–35] to facilitate the subsequent catalyst patterning for microfabricated fuel cells enabling their integration with active devices. The use of Nafion benefits the deposition process by solubilising the nanotubes and as a common constituent of fuel cells it is compatible with further utilisation of the composite in full cell operation.

2. Experimental methods

2.1. Materials

Multi-walled carbon nanotubes (Nanocyl®-3150) approximately 10 nm in diameter and 700 nm in length were supplied by Nanocyl™ (www.nanocyl.com). A Pt bath (Pt-DNS bath) based on 10 g Pt/litre was supplied by Metakem™ (www.metakem.com). Nafion perfluorinated ion-exchange resin (5 wt.%), sulphuric acid and methanol were supplied by Sigma–Aldrich. AAO circular membranes (Anodisc® 25) 2.5 cm in diameter, 60 μm thick, 200 nm pore size and 10^9 pore openings per cm^2 of membrane were supplied by Whatman™. p-Type Si wafers were supplied by MEMC Electronic Materials, Inc. Pt microdisc electrodes 10 μm diameter were supplied by Princeton Applied Research. The Pt counter electrode (2 cm in length, 1 mm diameter) and Ag/AgCl reference electrodes were supplied by IJ Cambria Scientific, Ltd.

2.2. In-house AAO formation

In-house AAO templates were fabricated on Si substrates to achieve smaller pore openings than those available with the commercial AAO templates using a method similar to those described in the literature [32–35]. Such AAO formation would enable the integration of the catalyst material for applications such as microfuel cell system on Si. The aluminium may also be prepatterned prior to anodisation or the blanket AAO may be patterned after processing to yield patterned templates for the catalyst deposition. In this work aluminium (1 μm) was sputter deposited on Pt wafer substrates fabricated as described earlier. Controlled anodisation created porous AAO templates presenting a honeycomb structure. During anodisation the Ti layer is also oxidised to titania, TiO_2. By controlling the voltage, acid concentration and temperature the pore diameter and percentage porosity of the resulting AAO could be tuned. Anodising at 2 °C at 40 V in 0.4 M oxalic acid generates 65 nm pores. Anodising at 2 °C at 20 V in 0.2 M H_2SO_4 generates 20 nm pores. Following anodisation, removal of titania and AAO barrier layers was effected by etching in 1% H_3PO_4—this serves to expose Pt at the base of the pores and leads to widening of the pore diameter. A general schematic of the process steps in the anodising of aluminium and Pt–CNT deposition is shown in Fig. 1.

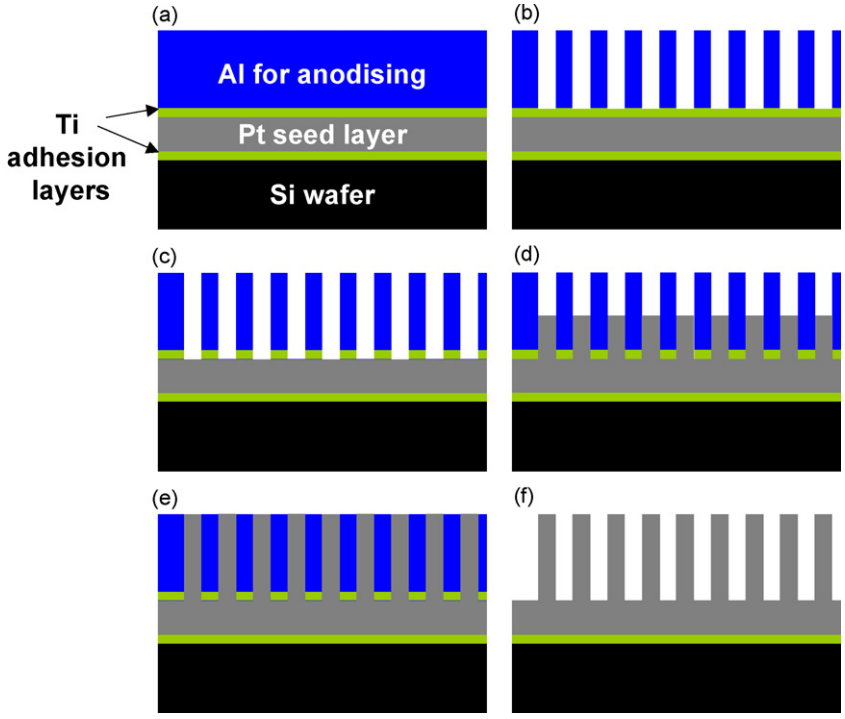

Fig. 1. Cross-sectional schematic showing the process for anodisation of alumina and Pt–CNT composite deposition therein. (a) Metal stack Al/Ti/Pt/Ti/in nm (1000/20/100/20) on standard p-type Si substrate (525 μm). (b) Porous anodised aluminium oxide (pore dimension 20–65 nm formed) as described in the text. (c) TiO_2 layer etch to expose Pt seed layer for Pt–CNT composite deposition. This structure is similar to that used for commercial AAO membranes onto which Ti adhesion and Pt seed layers were sputtered. (d) Pt–CNT composite electrodeposition in the porous template. (e) Pt–CNT deposition complete, in this case representing 1 μm long wires deposition in AAO. (f) AAO removed and Ti adhesion layer etch revealing Pt–CNT nanowires.

2.3. Electrochemical deposition of Pt–CNT composite

The MWNTs were dispersed in the Pt bath with the aid of Nafion. A dispersion of Pt–CNT/Nafion comprising 10 μg of CNT and 0.25 wt.% Nafion per ml. of Pt bath was prepared and sonicated for 10 min to afford a cloudy suspension. Sonication leads to shortening of the carbon nanotubes. Pt–CNT composite deposition was effected in a two-electrode cell with a target substrate designated as cathode and a Pt wire as anode under constant current conditions using a CH Instruments 660B electrochemical analyser. The bath was operated at 50 °C and 0.01 A cm^{-2} with an approximate deposition rate of 25 nm min^{-1}. For planar target substrates, 1 $in.^2$ sections of either Au or Pt wafers fabricated in-house were used. Au wafer substrates (100 nm Au layer deposited over 20 nm Cr adhesion layer) were fabricated using e-beam evaporation on p-type Si wafers (4 in. in diameter) and Pt wafer substrates (100 nm Pt layer deposited over 10 nm Ti adhesion layer) were fabricated using magnetron sputtering using a Nordiko 4000 series sputtering system on p-type Si wafers (4 in. in diameter). The Pt–CNT composites deposited thereon were 2D films, the thickness of which was determined by profilometry. In order to induce Pt–CNT composite deposition in the pores of Anodisc® 25 alumina membrane as target substrate the membrane was firstly made conducting by depositing 100 nm Pt with an underlying 10 nm Ti adhesion layer using e-beam evaporation. In order to ensure that composite deposition is restricted to the inside of the pores of the template, the coated Pt side is masked from the bath. For this a holder setup was employed. The alumina template was inserted between two 1 cm thick PTFE square plates of 4 cm side length, the lower plate was solid while the upper plate had a circular opening of 2.5 cm diameter which served to expose the template pores to the plating bath solution. A conducting Cu plate was sandwiched between the lower PTFE plate and the template. The template was inserted so that the Pt coated side is face down on the Cu plate thereby protecting it from the solution. An O-ring was positioned on the other side of the alumina template for added support before the two plates were secured together with four 0.5 cm diameter screws. The Pt–CNT composites deposited therein were 3D wires, the length of which was controlled by the deposition time and was measured using SEM and TEM.

2.4. Characterisation

SEM images of the composite array were recorded using a Hitachi S4000™ SEM at an acceleration voltage of 20 kV. Having deposited the composite in the pores, the alumina template was attached to a SEM conducting stub with an adhesive carbon sticker. The Pt backed side of the template was adhered to the adhesive carbon sticker. A few drops of 1 M sodium hydroxide were applied to the template for 40 min to allow for dissolution of the alumina. The solution was then removed and a few drops of water were applied to clean any residue from the template. As a final step the template was dried under a stream of nitrogen for 1 min. SEM images were recorded at 20 kV using Hitachi S4000™. To obtain TEM images of the Pt–CNT composite the alumina membrane with electrodeposited Pt–CNT composite nanowires was immersed in 1 M sodium hydroxide and sonicated for 5 min to release the composite from the template. The resulting residue was allowed to remain for 1 h in the 1 M sodium hydroxide solution to dissolve the porous alumina network. The residual nanowires are separated from the 1 M sodium hydroxide solution by centrifuging at 13,500 rpm for 10 min. The supernatant sodium hydroxide solution was removed and the nanowires were re-dispersed in deionised water to clean them. The aqueous dispersion was gently agitated before separating the nanowires by centrifuging at 13,500 rpm for 10 min. This cleaning step was repeated three times in total. Finally, the nanowires were dispersed in ethanol. A drop of the ethanolic solution was dropped on a carbon-coated Cu mesh TEM grid. The nanowires were imaged using JEOL 2000FX operating at accelerating voltage of 80 kV.

2.5. Electrochemical analysis

Cyclic voltammograms were recorded using a CH Instruments 660B electrochemical analyser. A three-electrode cell was used, the working electrode was a 10-μm Pt microdisc or Pt–CNT composite, the counter electrode was Pt and the reference electrode was Ag/AgCl. Cyclic voltammograms for 1 M methanol in 1 M sulphuric acid (−1.2 to 0.9 V vs. Ag/AgCl) were recorded at a scan rate of 20 mV s^{-1}.

3. Results and discussion

3.1. Microscopic analysis of deposit

The dispersion of MWNTs (10 nm diameter, ca. 700 nm long) in a commercial Pt plating bath was aided by the addition of Nafion. This solubilising agent afforded composite deposition with good adhesion to the Au substrates. Addition of pristine CNTs without any solubilising agent to a commercial Pt electroplating bath gave Pt–CNT deposits with poor adhesion to the Au substrate and showed impaired catalytic activity for methanol oxidation; the oxidation current at such composites was reduced to approximately 10% of that recorded at bare Pt electrodeposits without CNT reinforcement. The particular advantages of Nafion are the stable Teflon-type backbone which we expect to wrap the hydrophobic CNTs and the hydrophilic sulphonic acid end groups which facilitate the solubilisation in the aqueous solution. Pt–CNT composites were deposited at a current density of 0.01 A cm^{-2}, the resulting deposition rate is 25 nm min^{-1} and the typical voltage during deposition is −0.15 V. The optimum Pt–CNT-Nafion ratio in the plating bath for electrocatalytic activity towards methanol oxidation and minimum CO poisoning was determined to be 10 μg CNT/ml plating bath containing 0.25% (w/v) of Nafion. Planar Pt–CNT composites were deposited on a Au-wafer to a thickness of 560 nm in 22 min. Pt–CNT nanowire array composites were deposited in 200 nm Anodisc® AAO to afford nanowires 1 μm in length in 40 min.

Electron microscopy was utilised to analyse the composite deposit. The composite was deposited in 200 nm pore size Anodisc® AAO template to afford the Pt–CNT nanowire array shown in Fig. 2

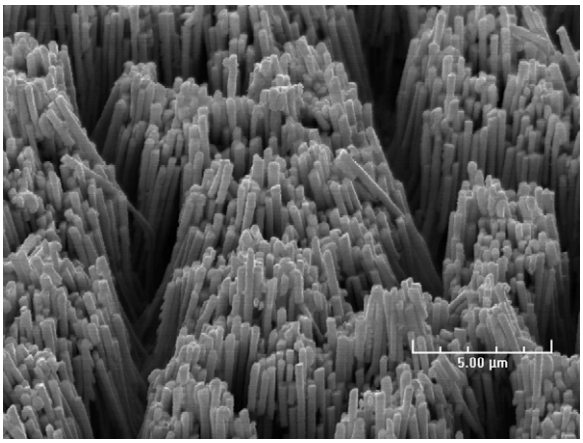

Fig. 2. SEM image of Pt–CNT nanowire composite array following dissolution of Anodisc® AAO template in which it was electrodeposited.

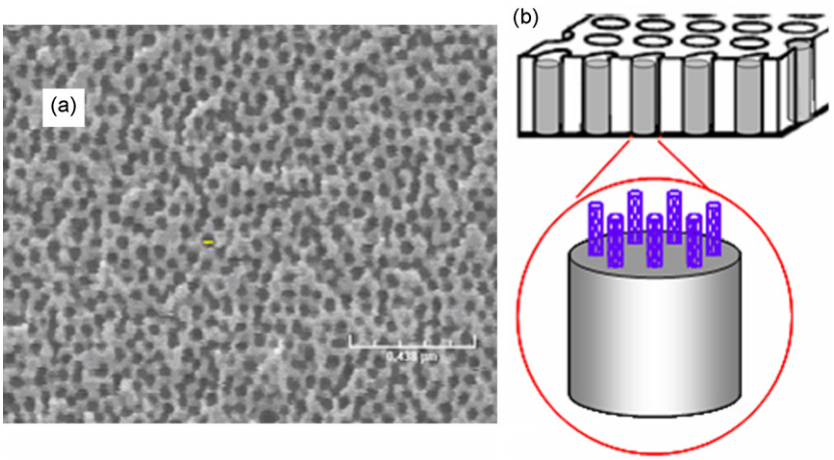

Fig. 3. (a) SEM image of AAO grown in oxalic acid on Si/Ti/Pt/Ti/Al wafer and (b) illustration of the AAO pore filling with Pt–CNT composite where the CNTs are aligned in the Pt host material.

following dissolution of the template. The composite was deposited in AAO templates such as that shown in Fig. 3a where 1 μm thick sputtered aluminium on Si was oxidised in 0.4 M oxalic acid to provide regular pores of approximately 65 nm in diameter. The schematic representation in Fig. 3b is based on the TEM image shown in Fig. 4 of an individual nanowire following dissolution of the AAO template membrane. This image clearly shows the 10 nm diameter MWNTs protruding from the end of the Pt host matrix. Interestingly these images indicate that the carbon nanotubes are aligned during deposition along the length of the Pt nanowire host.

It may be expected that the CNT wrapped in Nafion would align parallel to the sidewall of the AAO template during incorporation when the CNT and the pore size are of similar dimensions. This appears to be the case represented by the deposit in Fig. 4. Moreover, when CNTs are directionally aligned in a composite then the structure and properties of the composite are expected to be anisotropic, these include electrical conductivity, thermal conductivity, mechanical strength and coefficient of thermal expansion. It was shown that the electrical conductivity is anisotropic in aligned CNT-polymer composites [36] and aligned CNT-carbon composites [37] while anisotropic electrical and thermal transport properties were measured in magnetic field-aligned SWNTs [38].

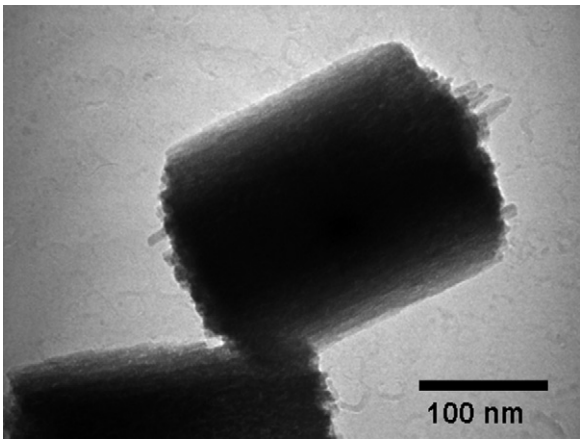

Fig. 4. TEM of individual Pt nanowire following dissolution of alumina membrane with CNT protrusions evident at both ends.

3.2. Methanol oxidation

The overall oxidation of methanol can be summarised as:

$$CH_3OH + H_2O \Rightarrow CO_2 + 6H^+ + 6e^- \quad (1)$$

It has been shown [39] that the initial reactions on a pure Pt electrode in acid involve the dissociative chemisorption of methanol to give Pt_3COH adsorbed species in a three-step process at $E < 0.5$ V vs. NHE:

$$CH_3OH + 2Pt \Rightarrow PtCH_2OH + PtH \quad (2a)$$

$$PtCHO_2H + 2Pt \Rightarrow Pt_2CHOH + PtH \quad (2b)$$

$$Pt_2CHOH + 2Pt \Rightarrow Pt_3COH + PtH \quad (2c)$$

The product of each step of Eq. (2) may react with OH_{ads} to yield different oxidation products, according to:

$$PtCH_2OH + OH_{ads} \Rightarrow Pt + H_2O + CH_2O \quad (3)$$

$$Pt_2CHOH + 2OH_{ads} \Rightarrow 2Pt + H_2O + HCOOH \quad (4)$$

$$Pt_3COH + 3OH_{ads} \Rightarrow 3Pt + 2H_2O + CO_2 \quad (5)$$

The formation of small amounts of formaldehyde and formic acid has been confirmed by some workers [40,41]. Over the potential range 0.5–1.1 V vs. NHE the following reaction occurs.

$$Pt_3COH \Rightarrow Pt_2CO + Pt + e^- \quad (6)$$

This may be followed by further oxidation according to the following equation:

$$Pt_2CO + OH_{ads} \Rightarrow PtCO_2H + Pt \quad (7a)$$

$$PtCO_2H + OH_{ads} \Rightarrow CO_2 + Pt + H_2O \quad (7b)$$

However, unreacted Pt_2CO can also rearrange (Eq. (8)) to give linearly bonded PtCO which acts as a poison:

$$Pt_2CO \Leftrightarrow PtCO + Pt \quad (8)$$

Reduction of $PtOH_{ads}$ according to Eq. (9) will uncover Pt surface atoms which can react with neighbouring PtCO according to the following equations:

$$PtOH_{ads} + H^+ + e^- \Leftrightarrow Pt + H_2O \quad (9)$$

$$PtCO + Pt \Leftrightarrow Pt_2CO \quad (10)$$

The poisoning carbonaceous species can be removed according to:

$$Pt_2CO + 2OH \Rightarrow 2Pt + H_2O + CO_2 \quad (11)$$

The total reaction involves a Langmuir–Hinshelwood type of reaction as summarised in the following equation:

$$PtCO + PtOH_{ads} \Leftrightarrow 2Pt + CO_2 + H^+ + e^- \quad (12)$$

The standard equilibrium potential for methanol oxidation according to Eq. (1) is 0.03 V vs. NHE, however, a significant reaction rate is not achieved until much higher potentials due to the difficulty in oxidation of intermediates which adsorb strongly on the Pt surface over a wide range of potentials, resulting in a poor activity towards methanol oxidation. This results in high oxidation overpotentials, usually far from the thermodynamic limit. Therefore, for commercial applications it is important to develop electrocatalysts tolerant to intermediate species. Good performance results have been obtained by combining Pt with oxophilic elements like Ru, Sn, Mo because in the latter, dissociation of water that produces OH surface groups, occurs at lower potentials than on Pt alone.

Methanol oxidation was found to be a surface structure-sensitive reaction and the activity of various monocrystalline Pt electrodes such as low-index basal planes and stepped surfaces as well as nanoparticles have been examined. The level of reactivity towards methanol decomposition of the three basal Pt planes increases in the order Pt(1 1 1) < Pt(1 0 0) < Pt(1 1 0) and the rate of methanol oxidation increases with the step density of Pt(1 1 1). The effect of steps on the product distribution during methanol oxidation was studied using differential electrochemical mass spectrometry (DEMS) at Pt(1 1 1) and Pt(3 2 2) [42]. It was shown that Pt (1 1 1) has a lower coverage of strongly adsorbed CO relative to smooth polycrystalline Pt and Pt(3 2 2). Savinova et al. examined the activity of electrodeposited Pt in the oxidation of methanol and CO_{ads} and found it to greatly exceed that for Pt(1 1 1), polycrystalline Pt or single-grained Pt particles [43]. They found that CO oxidation kinetics increases in the order Pt(1 1 1) < Pt(1 1 0) ≤ Pt (electrodeposited).

The oxidation response of 1 M methanol in 1 M H_2SO_4 at a 10-μm Pt microdisc (where the current is multiplied by 10) and at a Pt–CNT composite are shown in Fig. 5. The potential was scanned between −1.2 and 0.9 V vs. Ag/AgCl at a sweep rate of 20 mV s^{-1} at 25 °C. The onset of methanol oxidation is close to the onset of OH adsorption and the maximum oxidation rate corresponds to the transition from reversible to irreversible OH adsorption. The oxidation peak in the forward scan at a potential E_{fwd} corresponds to methanol oxidation while the oxidation peak in the reverse sweep at a potential E_{rev} is due to the removal of incompletely oxidised carbonaceous species formed in the forward sweep. The peak current on the forward sweep at the Pt microdisc shown in Fig. 5a is 2.5 mA cm^{-2} which is comparable to literature values, the current recorded for oxidation of 0.5 M methanol was 2.04 mA cm^{-2} at a 50-μm diameter Pt microdisc [44] and 1.47 mA cm^{-2} at polycrystalline Pt [45]. The more negative onset potential seen for methanol oxidation at the Pt–CNT composite, Fig. 5b, indicates a lower activation overpotential for methanol oxidation. The methanol oxidation current is 60 mA cm^{-2}. The oxidation peak for methanol, E_{fwd}, is observed at 0.56 and 0.63 V for the Pt–CNT composite and Pt microdisc, respectively. The more negative oxidation peak at the Pt–CNT composite suggests that methanol oxidation is energetically more favourable. The oxidation peak in the reverse scan E_{rev} is observed at a lower potential at the Pt–CNT composite (0.40 V) than at the Pt microdisc (0.56 V). The negative shift in potential indicates CO oxidation is energetically more favourable at the Pt–CNT composite than at Pt only.

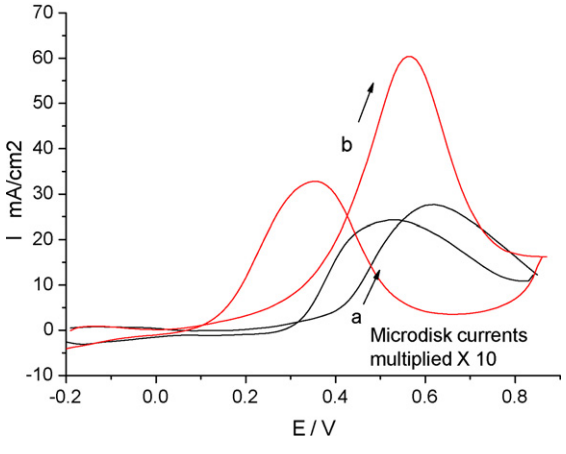

Fig. 5. Cyclic voltammograms (−1.2 to 0.9 V vs. Ag/AgCl) for 1 M methanol in 1 M sulphuric acid were recorded at a scan rate of 20 mV s^{-1} at (a) a Pt microdisc (– –) where the current is multiplied by 10 and (b) planar Pt–CNT composite (—) electrodeposited on a Au substrate.

The beneficial characteristics of the Pt–CNT composite were further enhanced when structured in a 200-nm pore size Anodisc® AAO template. The methanol oxidation current at the resulting Pt–CNT nanowire array composite was 73 mA cm^{-2}. The surface area and catalyst mass of the Pt–CNT nanowire array composite was estimated as follows. For a Pt–CNT deposit which is assumed to be cylindrical in shape with a height of 1 μm and radius of 100 nm, the corresponding volume is 3.142×10^{-14} cm^3 and Pt mass is 6.739×10^{-13} g (based on the density of Pt 21.45 g cm^{-3}). There are 10^9 pore openings per cm^2 of membrane and assuming 100% efficient Pt deposition the loading is 0.674 mg cm^{-2}, or 6.74 g m^{-2} which is an order of magnitude lower than recommended by commercial suppliers such as E-Tek USA. They recommend 50–80 wt.% Pt catalysts on high surface area carbon support Vulcan XC-72 (250 m^2 g^{-1}) for a DMFC where the Pt loading is 57–86 g m^{-2}. In estimating the active geometrical surface area for the composite formed in AAO it was assumed that only the outer disc-like faces of the nanowire array housed in the AAO template make contact with the solution. To compare with commercial Pt catalysts the current for 1 M methanol oxidation at 25 °C on 20 wt.% Pt on high surface area carbon support (Vulcan XC72R) reached 83 mA cm^{-2} at 73 mA mg^{-1} Pt mass activity [46]. Herein the current for 1 M methanol oxidation at a 1-μm Pt–CNT composite in 200 nm alumina pores at 25 °C and sweep rate of 20 mV s^{-1} reached a limiting current of 73 mA cm^{-2}, based on the Pt loading of 0.674 mg cm^{-2} the corresponding Pt mass activity is 108 mA mg^{-1}.

3.3. CO poisoning

It is generally accepted that CO species formed during methanol oxidation are the main reason for the slow kinetics of oxidation. Since CO species are the main poisoning intermediate a good catalyst for methanol oxidation should possess excellent CO electro-oxidising ability. Adsorbed CO poisons Pt and impedes further oxidation of methanol. The rate-determining step for CO_{ads} oxidation on Pt is an electrochemical or chemical reaction between CO_{ads} and OH according to Eq. (12). In the oxidation of methanol shown in Fig. 5 the ratio of the forward anodic peak current density (I_{fwd}) to the reverse anodic peak current density (I_{rev}), given by I_{fwd}/I_{rev}, provides a measure of the catalyst tolerance to carbonaceous species accumulation, in particular CO. A low I_{fwd}/I_{rev} ratio indicates poor oxidation of methanol to CO_2 during the anodic scan and excessive accumulation of carbonaceous residues on Pt. A high I_{fwd}/I_{rev} ratio represents the reverse case as more intermedi-

ate carbonaceous species are oxidised to CO_2 in the forward scan thus decreasing the extent of CO poisoning on Pt sites. The I_{fwd}/I_{rev} ratio increased from 1.14 for the Pt microdisc to 1.85 for the Pt–CNT composite indicating higher tolerance of the composite towards CO poisoning, as shown in Fig. 5. These results show that the electrodeposited Pt–CNT composite is viable for methanol oxidation. The reported I_{fwd}/I_{rev} ratio for the commercial E-TEK catalyst is 1.0 [46]. The ratio observed for nanoparticles of Pt on bundled CNTs is 1.4 [17]. Yang et al. demonstrated that the CO tolerance is higher for 3D Pt nanoparticle clusters with a fractal structure obtained by potential step electrodeposition on MWNTs than for 2D uniform Pt nanoparticle dispersion of MWNTs obtained by cyclic voltammetry [17]. The unique 3D 'flower like' structure of the Pt nanoparticle clusters on MWNTs has a higher electrochemically active surface area. The I_{fwd}/I_{rev} ratio was 2.0 for the 3D catalyst and 1.14 for the 2D catalyst. It was proposed that the peculiar shape of the nanoparticles in the 3D structure alters the types and number of facets, the number of atoms at corners or edges, the total number of atoms exposed on the surface and their coordination numbers.

CO oxidation is energetically more favourable at the Pt–CNT composite than at clean Pt as indicated by the negative shift in the oxidation potential. The negative potential shift could result from a lower density of adsorbed CO at the Pt–CNT composite. It was shown that adsorbed CO inhibits OH_{ads} generation and thus shifts CO oxidation to higher potentials [47]. It was demonstrated by Koper et al. [48] that the overpotential for CO oxidation is lowered at surfaces with a higher step density and is attributed to the preferential formation of oxygen-containing species at the step sites compared to terrace sites, the peak potential at Pt (5 3 3) was 0.17 V lower than that at Pt(1 1 1). Essentially, the activity towards CO oxidation is higher at surfaces with increased defect density. It was found by in situ infrared reflection–absorption spectroscopy that CO adsorbed on terraces is more reactive that CO adsorbed on steps. Initially OH_{ads} reacts with CO adsorbed in terraces, this is followed by the conversion of CO adsorbed on steps into 'terrace' CO and subsequent fast diffusion to the step sites. The negative shift in the potential for CO oxidation seen for the Pt–CNT composite may be further rationalised by comparison with the findings of Friedrich et al. [49] from their study of the dependence of CO stripping potential on Pt particle size. They showed that a negative shift in CO stripping potential (as seen at smaller particle sizes) is associated with either (a) a weaker CO bond, (b) increased CO diffusion or (c) faster generation of OH groups at the Pt surface.

Adsorbed H_2O or small amounts of adsorbed OH at lower potential are also widely considered to be necessary to remove CO intermediates. It was suggested by Arenz et.al [50,51] that CO-stripping at Pt particles is predominantly influenced by the ability of the surface to dissociate water and form OH_{ads} at defects or irregularities that act as active sites. They found that larger particles contain more irregularities than smaller ones resulting in greater ease of CO oxidation at the former. Investigation of CO oxidation at stepped Pt single crystal surfaces both in electrochemical environment and in UHV has proven that the formation of OH_{ads} species occurs preferentially at low coordinated sites such as steps and defects [43]. It is plausible that the incorporation of CNTs could prove beneficial in adsorbing H_2O to some extent. Irregularities or defects created in Pt upon introduction of CNTs can act as active sites for OH adsorption. The sonication of CNTs which promotes debundling results in shortening of CNTs and the formation of surface accessible oxidised species [28]. It is possible that carboxylate or carbonyl groups on the CNTs serve as 'active oxygen' for formation of CO_2 [52]. The CNTs protruding from the surface of Pt nanowires have oxide functional groups on their surface. Furthermore, the increased catalytic reactivity and lower self-poisoning ratios of the Pt–CNT composite may originate from other causes including more efficient mechanisms for the removal of the adsorbed species; increased electrical conductance of the MWNT when compared with the classical carbonaceous supports such as carbon black and the attainment of a preferred crystallographic orientation of Pt as a result of the interaction with the CNT as proposed by Guo et al. [53].

Two types of CO molecules were identified on Pt surfaces by Kinge et al. [54] in their study of the dependence of CO oxidation on Pt nanoparticle shape—one which is weakly bonded on kinetically controlled adsorbing sites on Pt(1 1 0) facets while the other is strongly bonded on thermodynamically controlled sites on Pt(1 1 1). It was noted that the electrodesorptive behaviour of CO depends on surface morphology, scan rate, oxygen content, potential limits and electrolyte composition. If adsorbed species are mobile on the surface then decreasing the scan rate during cyclic voltammetric experiments offers the system more time to relax allowing CO molecules move from oxidation sites of higher to lower energy if the measurement time is long enough to allow transfer to occur. A detailed investigation of the influence of scan rate was not performed in the current work.

3.4. CNT interaction

The higher electrocatalytic activities for methanol oxidation may be attributed to the unique 3D structure and electronic properties of Pt–CNT. The remarkable support effect of CNTs in Pt which enhance methanol oxidation may be related to a number of factors which include low charge transfer resistance at the CNT/electrolyte interface, presence of oxygen containing functional groups on the CNTs and a strong metal–support interaction in the Pt–CNT catalyst. Both surface and subsurface CNTs in the composite can promote enhanced kinetics of methanol oxidation owing to their rapid rate of electron transfer. CNTs in the immediate subsurface layer will alter the electronic environment of Pt atoms. Analysis of the strength of Pt–carbon support interactions using XPS [55] revealed that the binding energy of the Pt 4f doublet associated with metallic Pt increases in the order Pt-XC-72 < Pt-MWNTs < Pt-SWNTs. It was also shown that the relative amount of oxidised states of Pt increases in the order Pt-XC-72 < Pt-MWNTs < Pt-SWNTs. According to the bifunctional mechanism of methanol oxidation, the electrocatalytic activity is enhanced by the presence of PtO and PtO_2. A recent publication [56] has highlighted the benefit for methanol oxidation at a Pt catalyst deposited over a Pb support. They observed enhanced catalytic activity for methanol oxidation where the enhancement of the catalytic activity of Pt is attributed to an electronic effect of the underlayer on the Pt surface layer, affecting the extent of poison adsorption on the latter.

4. Conclusions

An array of Pt nanowires with vertically aligned CNTs embedded therein was fabricated using alumina templates. The described approach provides a simpler method for fabricating Pt–CNT composites as micro-fuel cell catalysts than growing CNTs on a metallic or carbon substrate followed by catalyst deposition. The purity of the composite electrodes is superior to those prepared by casting metal nanoparticle–CNT composites onto an electrode surface using a polymer binder as these can cause an increase in resistivity. The compromise between catalytic activity for methanol oxidation and CO adlayer oxidation seen for carbon-supported Pt nanoparticles [57] limits their efficiency as catalysts for DMFC applications and warrants further studies to explore the potential of this new catalyst material. The Pt–CNT composite has been shown to function as an improved methanol oxidation catalyst material

with enhanced carbon monoxide by-product tolerance. The relatively low peak potential for oxidation of 1 M methanol at the Pt–CNT composite at 0.56 V vs. Ag/AgCl indicates an energetically more favourable reaction. The Pt mass activity for the composite is 108 mA/mg and the CO tolerance is high based on the ratio I_{fwd}/I_{rev} of 1.85.

This process may allow for aligned CNT deposition in smaller template pores where the template pore and CNT diameter are of similar dimension (e.g. 10 nm CNT in 15–20 nm template), thereby decreasing the Pt content of the catalyst. The catalyst and patterning technique may be extended to oxidation of any carbon containing material such as glucose which demands better reliability, stability and high CO tolerance. The technique of co-depositing metal–CNT composite in nanoscale templates may be extended to other metals for applications such as aligned Cu–CNT composite for integrated circuit interconnects. The composite catalyst may also be deposited as nanoscale thin films over a templated electrically conducting support material such as Cu [58]. The approach affords a composite with directionally aligned CNTs in Pt; the CNTs align vertically along the axis of the Pt nanowires to give an anisotropic structure. The process can be extended to include the fabrication of a range of aligned CNT/metal(alloy) composites with anisotropic properties.

Acknowledgement

This work was supported by the Enterprise Ireland Proof of Concept Grant no. PC/2005/033.

References

[1] A. Kundu, J.H. Jang, J.H. Gi, C.R. Jung, H.R. Lee, S.-H. Kim, B. Ku, Y.S. Oh, J. Power Sources 170 (2007) 67.
[2] G.Q. Lu, C.Y. Wang, T.J. Yen, X. Zhang, Electrochim. Acta 49 (2004) 821.
[3] T.J. Yen, N. Fang, X. Zhang, G.Q. Lu, C.Y. Wang, Appl. Phys. Lett. 83 (2003) 4056.
[4] J.S. Wainright, R.F. Savinell, C.C. Liu, M. Litt, Electrochim. Acta 48 (2003) 2869.
[5] S.J. Lee, A. Chang-Chien, S.W. Cha, R. O'Hayre, Y.I. Park, Y. Saito, F.B. Prinz, J. Power Sources 112 (2002) 410.
[6] R. Hahn, S. Wagner, A. Schmitz, H. Reichl, J. Power Sources 131 (2004) 73.
[7] H. Liu, C. Song, L. Zhang, J. Zhang, H. Wang, D.P. Wilkinson, J. Power Sources 155 (2006) 95.
[8] G. Girishkumar, K. Vinodgopal, P.V. Kamat, J. Phys. Chem. B 108 (2004) 19960.
[9] Z. He, J. Chen, D. Liu, H. Tang, W. Deng, Y. Kuang, Mater. Chem. Phys. 85 (2004) 396.
[10] M.-C. Tsai, T.-K. Yeh, C.-H. Tsai, Electrochem. Commun. 8 (2006) 1445.
[11] T. Matsumoto, T. Komatsu, H. Nakano, K. Arai, Y. Nagashima, E. Yoo, T. Yamazaki, M. Kijima, H. Shimizu, Y. Takasawa, J. Nakamura, Catal. Today 90 (2004) 277.
[12] B. Rajesh, V. Karthik, S. Karthikeyan, K. Ravindranathan Thampi, J.-M. Bonard, B. Viswanathan, Fuel 81 (2002) 2177.
[13] H. Tang, J. Chen, S. Yao, L. Nie, Y. Kuang, Z. Huang, D. Wang, Z. Ren, Mater. Chem. Phys. 92 (2005) 548.
[14] J. Narayanamoorthy, S. Durairaij, Y. Song, Y. Xu, J. Choi, Appl. Phys. Lett. 90 (2007) 063112.
[15] G. Zhao, J. He, C. Zhang, J. Zhou, X. Chen, T. Wang, J. Phys. Chem. C 112 (2008) 1028.
[16] Y. Liang, J. Li, S. Wang, X. Fu, Q. Xu, J. Lin, D. Liao, Catal. Lett. 120 (2008) 236.
[17] S. Yang, Y. Zhao, H. Zhong, Y. Li, Adv. Funct. Mater. 17 (2007) 1537.
[18] G. Girishkumar, M. Rettker, R. Underhile, D. Binz, K. Vinodgopal, P. McGinn, P.V. Kamat, Langmuir 21 (2005) 8487.
[19] G. Che, B.B. Lakshmi, C.R. Martin, E.R. Fisher, Langmuir 15 (1999) 750.
[20] J.-B. He, C.-L. Chen, J.-H. Liu, Sens. Actuators B: Chem. 99 (2004) 1.
[21] X.H. Chen, F.Q. Cheng, S.L. Li, L.P. Zhou, D.Y. Li, Surf. Coat. Technol. 155 (2002) 274.
[22] K.T. Kim, S.I. Cha, S.H. Hong, Mater. Sci. Eng. A: Struct. 449–451 (2007) 46.
[23] S. Arai, M. Endo, T. Sato, A. Koide, Electrochem. Solid State 9 (2006) C131.
[24] Y. Cho, G. Choi, D. Kim, Electrochem. Solid State 9 (2006) G107.
[25] M.J. O'Connell, P. Boul, L.M. Ericson, C. Huffman, Y. Wang, E. Haroz, C. Kuper, J. Tour, K.D. Ausman, R.E. Smalley, Chem. Phys. Lett. 342 (2001) 265.
[26] S. Arai, M. Endo, Electrochem. Commun. 5 (2003) 797.
[27] J. Wang, M. Musameh, Y. Lin, J. Am. Chem. Soc. 125 (2003) 2408.
[28] J. Tkac, T. Ruzgas, Electrochem. Commun. 8 (2006) 899.
[29] C. Engtrakul, M.F. Davis, T. Gennett, A.C. Dillon, K.M. Jones, M.J. Heben, J. Am. Chem. Soc. 127 (2005) 17548.
[30] J.-H. Lee, U. Paik, J.-Y. Choi, K.K. Kim, S.-M. Yoon, J. Lee, B.-K. Kim, J.M. Kim, M.H. Park, C.W. Yang, K.H. An, Y.H. Lee, J. Phys. Chem. C 111 (2007) 2477.
[31] A.Y. Kasumov, H. Bouchiat, B. Reulet, O. Stephan, I.I. Khodos, Y.B. Gorbatov, C. Colliex, Europhys. Lett. 43 (1998) 89.
[32] M.S. Sander, L.-S. Tan, Adv. Funct. Mater. 13 (2003) 393.
[33] E.S. Kooij, H. Wormeester, A.C. Gâlcâ, B. Poelsema, Electrochem. Solid State 6 (2003) B52.
[34] M.M. Crouse, A.E. Miller, D.T. Crouse, A.A. Ikram, J. Electrochem. Soc 152 (2005) D167.
[35] N. Yasui, A. Imada, T. Den, Appl. Phys. Lett. 83 (2003) 3347.
[36] H. Huang, C.H. Liu, Y. Wu, S. Fan, Adv. Mater. 17 (2005) 1652.
[37] Q. Gong, Z. Li, D. Li, X. Bai, J. Liang, Solid State Commun. 131 (2004) 399.
[38] J. Hone, M.C. Llaguno, N.M. Nemes, A.T. Johnson, J.E. Fischer, D.A. Walters, M.J. Casavant, J. Schmidt, R.E. Smalley, Appl. Phys. Lett. 77 (2000) 666.
[39] R. Manoharan, J.B. Goodenough, J. Mater. Chem 2 (1992) 875.
[40] H. Wang, T. Loeffler, H. Baltruschat, J. Appl. Electrochem. 21 (2001) 759.
[41] E.A. Batista, G.R.P. Malpass, A.J. Motheo, T. Iwasita, J. Electroanal. Chem. 571 (2004) 273.
[42] H. Wang, H. Baltruschat, J. Phys. Chem. C 111 (2007) 7038.
[43] E.R. Savinova, O.V. Cherstiouk, A.N. Gavrilov, I.Y. Molina, G.A. Tsirlina, L.M. Plyasova, J. Solid State Electrochem. 12 (2008) 497.
[44] M. Umeda, M. Kokubo, M. Mohamedi, I. Uchida, Electrochim. Acta 48 (2003) 1367.
[45] W. Xu, T. Lu, C. Liu, W. Xing, J. Phys. Chem. B 109 (2005) 7872.
[46] V. Raghuveer, A. Manthiram, J. Electrochem. Soc. 152 (2005) A1504.
[47] Z. Jusys, R.J. Behm, J. Phys. Chem. B 105 (2001) 10874.
[48] S.C.S. Lai, N.P. Lebedeva, T.H.M. Housmans, M.T.M. Koper, Top. Catal. 46 (2007) 320.
[49] K.A. Friedrich, F. Henglein, W. Unkauf, Electrochim. Acta 47 (2001) 689.
[50] M. Arenz, P.N. Ross, N.M. Markovic, J. Am. Chem. Soc. 127 (2005) 6819.
[51] M. Arenz, P.N. Ross, N.M. Markovic, K.J.J. Mayrhofer, B. Blizanac, V. Stamenkovic, Electrochim. Acta 50 (2005) 5144.
[52] D. Guo, H.L. Li, J. Electroanal. Chem. 573 (2004) 197.
[53] D. Guo, H. Li, J. Power Sources 160 (2006) 44.
[54] S. Kinge, H. Bommemann, Appl. Organometall. Chem. 22 (2008) 49.
[55] G. Wu, Y. Chen, B. Xu, Electrochem. Commun. 7 (2005) 1237.
[56] S. Papadimitriou, A. Tegou, E. Pavlidou, G. Kokkinidis, S. Sotiropoulos, Electrochim. Acta 52 (2007) 6254.
[57] D.E. Nikles, E. Ada, Z. Liu, J. Power Sources 164 (2007) 472.
[58] P.L. Taberna, S. Mitra, P. Poizot, P. Simon, J.-M. Tarascon, Nat. Mater. 5 (2006) 567.